PHYSICAL REVIEW D **85,** 012002 (2012)

Search for $WZ+ZZ$ production with missing transverse energy+jets with b enhancement at $\sqrt{s}=1.96$ TeV

T. Aaltonen,[21] B. Álvarez González,[10,x] S. Amerio,[42] D. Amidei,[33] A. Anastassov,[37] A. Annovi,[18] J. Antos,[13] G. Apollinari,[16]
J. A. Appel,[16] A. Apresyan,[51] T. Arisawa,[63] A. Artikov,[14] J. Asaadi,[57] W. Ashmanskas,[16] B. Auerbach,[66] A. Aurisano,[57]
F. Azfar,[41] W. Badgett,[16] A. Barbaro-Galtieri,[27] V. E. Barnes,[51] B. A. Barnett,[24] P. Barria,[46,48] P. Bartos,[13] M. Bauce,[42,43]
G. Bauer,[31] F. Bedeschi,[46] D. Beecher,[29] S. Behari,[24] G. Bellettini,[46,47] J. Bellinger,[65] D. Benjamin,[15] A. Beretvas,[16]
A. Bhatti,[53] M. Binkley,[16,a] D. Bisello,[42,43] I. Bizjak,[29,bb] K. R. Bland,[5] B. Blumenfeld,[24] A. Bocci,[15] A. Bodek,[52]
D. Bortoletto,[51] J. Boudreau,[50] A. Boveia,[12] L. Brigliadori,[6,7] A. Brisuda,[13] C. Bromberg,[34] E. Brucken,[22]
M. Bucciantonio,[46,47] J. Budagov,[14] H. S. Budd,[52] S. Budd,[23] K. Burkett,[16] G. Busetto,[42,43] P. Bussey,[20] A. Buzatu,[32]
C. Calancha,[30] S. Camarda,[4] M. Campanelli,[29] M. Campbell,[33] F. Canelli,[12,16] B. Carls,[23] D. Carlsmith,[65] R. Carosi,[46]
S. Carrillo,[17,l] S. Carron,[16] B. Casal,[10] M. Casarsa,[16] A. Castro,[6,7] P. Catastini,[21] D. Cauz,[58] V. Cavaliere,[23] M. Cavalli-Sforza,[4]
A. Cerri,[27,f] L. Cerrito,[29,r] Y. C. Chen,[1] M. Chertok,[8] G. Chiarelli,[46] G. Chlachidze,[16] F. Chlebana,[16] K. Cho,[26] D. Chokheli,[14]
J. P. Chou,[21] W. H. Chung,[65] Y. S. Chung,[52] C. I. Ciobanu,[44] M. A. Ciocci,[46,48] A. Clark,[19] C. Clarke,[64] G. Compostella,[42,43]
M. E. Convery,[16] J. Conway,[8] M. Corbo,[44] M. Cordelli,[18] C. A. Cox,[8] D. J. Cox,[8] F. Crescioli,[46,47] C. Cuenca Almenar,[66]
J. Cuevas,[10,x] R. Culbertson,[16] D. Dagenhart,[16] N. d'Ascenzo,[44,v] M. Datta,[16] P. de Barbaro,[52] S. De Cecco,[54] G. De Lorenzo,[4]
M. Dell'Orso,[46,47] C. Deluca,[4] L. Demortier,[53] J. Deng,[15,c] M. Deninno,[6] F. Devoto,[22] M. d'Errico,[42,43] A. Di Canto,[46,47]
B. Di Ruzza,[46] J. R. Dittmann,[5] M. D'Onofrio,[28] S. Donati,[46,47] P. Dong,[16] M. Dorigo,[58] T. Dorigo,[42] K. Ebina,[63] A. Elagin,[57]
A. Eppig,[33] R. Erbacher,[8] D. Errede,[23] S. Errede,[23] N. Ershaidat,[44,aa] R. Eusebi,[57] H. C. Fang,[27] S. Farrington,[41] M. Feindt,[25]
J. P. Fernandez,[30] C. Ferrazza,[46,49] R. Field,[17] G. Flanagan,[51,t] R. Forrest,[8] M. J. Frank,[5] M. Franklin,[21] J. C. Freeman,[16]
Y. Funakoshi,[63] I. Furic,[17] M. Gallinaro,[53] J. Galyardt,[11] J. E. Garcia,[19] A. F. Garfinkel,[51] P. Garosi,[46,48] H. Gerberich,[23]
E. Gerchtein,[16] S. Giagu,[54,55] V. Giakoumopoulou,[3] P. Giannetti,[46] K. Gibson,[50] C. M. Ginsburg,[16] N. Giokaris,[3] P. Giromini,[18]
M. Giunta,[46] G. Giurgiu,[24] V. Glagolev,[14] D. Glenzinski,[16] M. Gold,[36] D. Goldin,[57] N. Goldschmidt,[17] A. Golossanov,[16]
G. Gomez,[10] G. Gomez-Ceballos,[31] M. Goncharov,[31] O. González,[30] I. Gorelov,[36] A. T. Goshaw,[15] K. Goulianos,[53]
S. Grinstein,[4] C. Grosso-Pilcher,[12] R. C. Group,[62,16] J. Guimaraes da Costa,[21] Z. Gunay-Unalan,[34] C. Haber,[27] S. R. Hahn,[16]
E. Halkiadakis,[50] A. Hamaguchi,[39] J. Y. Han,[47] F. Happacher,[17] K. Hara,[53] D. Hare,[56] M. Hare,[61] R. F. Harr,[64] K. Hatakeyama,[5]
C. Hays,[41] M. Heck,[25] J. Heinrich,[45] M. Herndon,[65] S. Hewamanage,[5] D. Hidas,[56] A. Hocker,[16] W. Hopkins,[16,g] D. Horn,[25]
S. Hou,[1] R. E. Hughes,[38] M. Hurwitz,[12] U. Husemann,[66] N. Hussain,[32] M. Hussein,[34] J. Huston,[34] G. Introzzi,[46] M. Iori,[55,54]
A. Ivanov,[8,p] E. James,[16] D. Jang,[11] B. Jayatilaka,[15] E. J. Jeon,[26] M. K. Jha,[6] S. Jindariani,[16] W. Johnson,[8] M. Jones,[51]
K. K. Joo,[26] S. Y. Jun,[11] T. R. Junk,[16] T. Kamon,[57] P. E. Karchin,[64] A. Kasmi,[5] Y. Kato,[40,o] W. Ketchum,[12] J. Keung,[45]
V. Khotilovich,[57] B. Kilminster,[16] D. H. Kim,[26] H. S. Kim,[26] H. W. Kim,[26] J. E. Kim,[26] M. J. Kim,[18] S. B. Kim,[26] S. H. Kim,[60]
Y. K. Kim,[12] N. Kimura,[63] M. Kirby,[15] S. Klimenko,[17] K. Kondo,[63] D. J. Kong,[26] J. Konigsberg,[17] A. V. Kotwal,[15] M. Kreps,[25]
J. Kroll,[45] D. Krop,[12] N. Krumnack,[5,m] M. Kruse,[15] V. Krutelyov,[57,d] T. Kuhr,[25] M. Kurata,[60] S. Kwang,[12] A. T. Laasanen,[51]
S. Lami,[46] S. Lammel,[16] M. Lancaster,[29] R. L. Lander,[8] K. Lannon,[38,w] A. Lath,[56] G. Latino,[47,46] T. LeCompte,[2] E. Lee,[57]
H. S. Lee,[12] J. S. Lee,[26] S. W. Lee,[57,y] S. Leo,[47,46] S. Leone,[46] J. D. Lewis,[16] A. Limosani,[15,s] C.-J. Lin,[26] J. Linacre,[41]
M. Lindgren,[16] E. Lipeles,[45] A. Lister,[19] D. O. Litvintsev,[16] C. Liu,[50] Q. Liu,[51] T. Liu,[16] S. Lockwitz,[66] A. Loginov,[66]
D. Lucchesi,[42,41] J. Lueck,[25] P. Lujan,[27] P. Lukens,[16] G. Lungu,[53] J. Lys,[27] R. Lysak,[13] R. Madrak,[16] K. Maeshima,[16]
K. Makhoul,[31] S. Malik,[53] G. Manca,[28,b] A. Manousakis-Katsikakis,[3] F. Margaroli,[51] C. Marino,[25] M. Martínez,[4]
R. Martínez-Ballarín,[30] P. Mastrandrea,[54] M. E. Mattson,[64] P. Mazzanti,[6] K. S. McFarland,[52] P. McIntyre,[57] R. McNulty,[28,j]
A. Mehta,[28] P. Mehtala,[22] A. Menzione,[46] C. Mesropian,[53] T. Miao,[16] D. Mietlicki,[33] A. Mitra,[1] H. Miyake,[60] S. Moed,[21]
N. Moggi,[6] M. N. Mondragon,[16,l] C. S. Moon,[26] R. Moore,[16] M. J. Morello,[16] J. Morlock,[25] P. Movilla Fernandez,[16]
A. Mukherjee,[16] Th. Muller,[25] P. Murat,[16] M. Mussini,[7,6] J. Nachtman,[16,n] Y. Nagai,[60] J. Naganoma,[63] I. Nakano,[39] A. Napier,[61]
J. Nett,[57] C. Neu,[62] M. S. Neubauer,[23] J. Nielsen,[27,e] L. Nodulman,[2] O. Norniella,[23] E. Nurse,[29] L. Oakes,[41] S. H. Oh,[15]
Y. D. Oh,[26] I. Oksuzian,[62] T. Okusawa,[40] R. Orava,[22] L. Ortolan,[4] S. Pagan Griso,[42,43] C. Pagliarone,[58] E. Palencia,[10,f]
V. Papadimitriou,[16] A. A. Paramonov,[2] J. Patrick,[16] G. Pauletta,[59,58] M. Paulini,[11] C. Paus,[31] D. E. Pellett,[8] A. Penzo,[58]
T. J. Phillips,[15] G. Piacentino,[46] E. Pianori,[45] J. Pilot,[38] K. Pitts,[23] C. Plager,[9] L. Pondrom,[65] S. Poprocki,[16,g] K. Potamianos,[51]
O. Poukhov,[14] F. Prokoshin,[14,z] A. Pranko,[27] F. Ptohos,[18,h] E. Pueschel,[11] G. Punzi,[47,46] J. Pursley,[65] A. Rahaman,[50]
V. Ramakrishnan,[65] N. Ranjan,[51] I. Redondo,[30] P. Renton,[41] M. Rescigno,[54] T. Riddick,[29] F. Rimondi,[7,6] L. Ristori,[46,16]
A. Robson,[20] T. Rodrigo,[10] T. Rodriguez,[45] E. Rogers,[23] S. Rolli,[61,i] R. Roser,[16] M. Rossi,[58] F. Rubbo,[16] F. Ruffini,[48,46]
A. Ruiz,[10] J. Russ,[11] V. Rusu,[16] A. Safonov,[57] W. K. Sakumoto,[52] Y. Sakurai,[63] L. Santi,[59,58] L. Sartori,[46] K. Sato,[60]
V. Saveliev,[44,v] A. Savoy-Navarro,[44] P. Schlabach,[16] A. Schmidt,[25] E. E. Schmidt,[16] M. P. Schmidt,[66] M. Schmitt,[37]

1550-7998/2012/85(1)/012002(10)

T. Schwarz,[8] L. Scodellaro,[10] A. Scribano,[48,46] F. Scuri,[46] A. Sedov,[51] S. Seidel,[36] Y. Seiya,[40] A. Semenov,[14] F. Sforza,[47,46] A. Sfyrla,[23] S. Z. Shalhout,[8] T. Shears,[28] P. F. Shepard,[50] M. Shimojima,[60,u] S. Shiraishi,[12] M. Shochet,[12] I. Shreyber,[35] A. Simonenko,[14] P. Sinervo,[32] A. Sissakian,[13] K. Sliwa,[61] J. R. Smith,[8] F. D. Snider,[16] A. Soha,[16] S. Somalwar,[56] V. Sorin,[4] P. Squillacioti,[46] M. Stancari,[16] M. Stanitzki,[66] R. St. Denis,[20] B. Stelzer,[32] O. Stelzer-Chilton,[32] D. Stentz,[37] J. Strologas,[36] G. L. Strycker,[32] Y. Sudo,[60] A. Sukhanov,[17] I. Suslov,[14] K. Takemasa,[60] Y. Takeuchi,[60] J. Tang,[12] M. Tecchio,[33] P. K. Teng,[1] J. Thom,[16,g] J. Thome,[11] G. A. Thompson,[23] E. Thomson,[45] P. Ttito-Guzmán,[30] S. Tkaczyk,[16] D. Toback,[57] S. Tokar,[13] K. Tollefson,[34] T. Tomura,[60] D. Tonelli,[16] S. Torre,[18] D. Torretta,[16] P. Totaro,[42] M. Trovato,[49,46] Y. Tu,[45] F. Ukegawa,[60] S. Uozumi,[26] A. Varganov,[33] F. Vázquez,[17,l] G. Velev,[15] C. Vellidis,[3] M. Vidal,[30] I. Vila,[10] R. Vilar,[10] J. Vizán,[10] M. Vogel,[36] G. Volpi,[47,46] P. Wagner,[45] R. L. Wagner,[16] T. Wakisaka,[40] R. Wallny,[9] S. M. Wang,[1] A. Warburton,[32] D. Waters,[29] M. Weinberger,[57] W. C. Wester III,[16] B. Whitehouse,[61] D. Whiteson,[45,c] A. B. Wicklund,[2] E. Wicklund,[16] S. Wilbur,[12] F. Wick,[25] H. H. Williams,[45] J. S. Wilson,[38] P. Wilson,[16] B. L. Winer,[38] P. Wittich,[16,g] S. Wolbers,[16] H. Wolfe,[38] T. Wright,[33] X. Wu,[19] Z. Wu,[5] K. Yamamoto,[40] J. Yamaoka,[15] T. Yang,[16] U. K. Yang,[12,q] Y. C. Yang,[26] W.-M. Yao,[27] G. P. Yeh,[16] K. Yi,[16,n] J. Yoh,[16] K. Yorita,[63] T. Yoshida,[40,k] G. B. Yu,[15] I. Yu,[26] S. S. Yu,[16] J. C. Yun,[16] A. Zanetti,[58] Y. Zeng,[15] and S. Zucchelli[7,6]

(CDF Collaboration)

[1]*Institute of Physics, Academia Sinica, Taipei, Taiwan 11529, Republic of China*
[2]*Argonne National Laboratory, Argonne, Illinois 60439, USA*
[3]*University of Athens, 157 71 Athens, Greece*
[4]*Institut de Fisica d'Altes Energies, ICREA, Universitat Autonoma de Barcelona, E-08193, Bellaterra (Barcelona), Spain*
[5]*Baylor University, Waco, Texas 76798, USA*
[6]*Istituto Nazionale di Fisica Nucleare Bologna, University of Bologna, I-40127 Bologna, Italy*
[7]*Istituto Nazionale di Fisica Nucleare Bologna, University of Bologna, I-40127 Bologna, Italy*
[8]*University of California, Davis, Davis, California 95616, USA*
[9]*University of California, Los Angeles, Los Angeles, California 90024, USA*
[10]*Instituto de Fisica de Cantabria, CSIC-University of Cantabria, 39005 Santander, Spain*
[11]*Carnegie Mellon University, Pittsburgh, Pennsylvania 15213, USA*
[12]*Enrico Fermi Institute, University of Chicago, Chicago, Illinois 60637, USA*
[13]*Comenius University, 842 48 Bratislava, Slovakia; Institute of Experimental Physics, 040 01 Kosice, Slovakia*
[14]*Joint Institute for Nuclear Research, RU-141980 Dubna, Russia*
[15]*Duke University, Durham, North Carolina 27708, USA*
[16]*Fermi National Accelerator Laboratory, Batavia, Illinois 60510, USA*
[17]*University of Florida, Gainesville, Florida 32611, USA*
[18]*Laboratori Nazionali di Frascati, Istituto Nazionale di Fisica Nucleare, I-00044 Frascati, Italy*
[19]*University of Geneva, CH-1211 Geneva 4, Switzerland*
[20]*Glasgow University, Glasgow G12 8QQ, United Kingdom*
[21]*Harvard University, Cambridge, Massachusetts 02138, USA*
[22]*Division of High Energy Physics, Department of Physics, University of Helsinki*
and Helsinki Institute of Physics, FIN-00014, Helsinki, Finland
[23]*University of Illinois, Urbana, Illinois 61801, USA*
[24]*The Johns Hopkins University, Baltimore, Maryland 21218, USA*
[25]*Institut für Experimentelle Kernphysik, Karlsruhe Institute of Technology, D-76131 Karlsruhe, Germany*
[26]*Center for High Energy Physics: Kyungpook National University, Daegu 702-701, Korea;*
Seoul National University, Seoul 151-742, Korea; Sungkyunkwan University, Suwon 440-746, Korea;
Korea Institute of Science and Technology Information, Daejeon 305-806, Korea;
Chonnam National University, Gwangju 500-757, Korea; Chonbuk National University, Jeonju 561-756, Korea
[27]*Ernest Orlando Lawrence Berkeley National Laboratory, Berkeley, California 94720, USA*
[28]*University of Liverpool, Liverpool L69 7ZE, United Kingdom*
[29]*University College London, London WC1E 6BT, United Kingdom*
[30]*Centro de Investigaciones Energeticas Medioambientales y Tecnologicas, E-28040 Madrid, Spain*
[31]*Massachusetts Institute of Technology, Cambridge, Massachusetts 02139, USA*
[32]*Institute of Particle Physics: McGill University, Montréal, Québec, Canada H3A 2T8;*
Simon Fraser University, Burnaby, British Columbia, Canada V5A 1S6;
University of Toronto, Toronto, Ontario, Canada M5S 1A7;
and TRIUMF, Vancouver, British Columbia, Canada V6T 2A3
[33]*University of Michigan, Ann Arbor, Michigan 48109, USA*
[34]*Michigan State University, East Lansing, Michigan 48824, USA*
[35]*Institution for Theoretical and Experimental Physics, ITEP, Moscow 117259, Russia*

[36]*University of New Mexico, Albuquerque, New Mexico 87131, USA*
[37]*Northwestern University, Evanston, Illinois 60208, USA*
[38]*The Ohio State University, Columbus, Ohio 43210, USA*
[39]*Okayama University, Okayama 700-8530, Japan*
[40]*Osaka City University, Osaka 588, Japan*
[41]*University of Oxford, Oxford OX1 3RH, United Kingdom*
[42]*Istituto Nazionale di Fisica Nucleare, Sezione di Padova-Trento, I-35131 Padova, Italy*
[43]*University of Padova, I-35131 Padova, Italy*
[44]*LPNHE, Universite Pierre et Marie Curie/IN2P3-CNRS, UMR7585, Paris, F-75252 France*
[45]*University of Pennsylvania, Philadelphia, Pennsylvania 19104, USA*
[46]*Istituto Nazionale di Fisica Nucleare Pisa, I-56127 Pisa, Italy*
[47]*University of Pisa, I-56127 Pisa, Italy*
[48]*University of Siena, I-56127 Pisa, Italy*
[49]*Scuola Normale Superiore, I-56127 Pisa, Italy*
[50]*University of Pittsburgh, Pittsburgh, Pennsylvania 15260, USA*
[51]*Purdue University, West Lafayette, Indiana 47907, USA*
[52]*University of Rochester, Rochester, New York 14627, USA*
[53]*The Rockefeller University, New York, New York 10065, USA*
[54]*Istituto Nazionale di Fisica Nucleare, Sezione di Roma 1, I-00185 Roma, Italy*
[55]*Sapienza Università di Roma, I-00185 Roma, Italy*
[56]*Rutgers University, Piscataway, New Jersey 08855, USA*
[57]*Texas A&M University, College Station, Texas 77843, USA*
[58]*Istituto Nazionale di Fisica Nucleare Trieste/Udine, I-34100 Trieste, I-33100 Udine, Italy*
[59]*University of Udine, I-33100 Udine, Italy*
[60]*University of Tsukuba, Tsukuba, Ibaraki 305, Japan*
[61]*Tufts University, Medford, Massachusetts 02155, USA*
[62]*University of Virginia, Charlottesville, Virginia 22906, USA*
[63]*Waseda University, Tokyo 169, Japan*
[64]*Wayne State University, Detroit, Michigan 48201, USA*
[65]*University of Wisconsin, Madison, Wisconsin 53706, USA*
[66]*Yale University, New Haven, Connecticut 06520, USA*

(Received 11 August 2011; published 6 January 2012)

---

[a] Deceased
[b] Visitor from Istituto Nazionale di Fisica Nucleare, Sezione di Cagliari, 09042 Monserrato (Cagliari), Italy
[c] Visitor from University of CA Irvine, Irvine, CA 92697, USA
[d] visitor from University of CA Santa Barbara, Santa Barbara, CA 93106, USA
[e] Visitor from University of CA Santa Cruz, Santa Cruz, CA 95064, USA
[f] Visitor from CERN,CH-1211 Geneva, Switzerland
[g] Visitor from Cornell University, Ithaca, NY 14853, USA
[h] Visitor from University of Cyprus, Nicosia CY-1678, Cyprus
[i] Visitor from Office of Science, U.S. Department of Energy, Washington, DC 20585, USA
[j] Visitor from University College Dublin, Dublin 4, Ireland
[k] Visitor from University of Fukui, Fukui City, Fukui Prefecture, Japan 910-0017
[l] Visitor from Universidad Iberoamericana, Mexico D.F., Mexico
[m] Visitor from Iowa State University, Ames, IA 50011, USA
[n] Visitor from University of Iowa, Iowa City, IA 52242, USA
[o] Visitor from Kinki University, Higashi-Osaka City, Japan 577-8502
[p] Visitor from Kansas State University, Manhattan, KS 66506, USA
[q] Visitor from University of Manchester, Manchester M13 9PL, United Kingdom
[r] Visitor from Queen Mary, University of London, London, E1 4NS, United Kingdom
[s] Visitor from University of Melbourne, Victoria 3010, Australia
[t] Visitor from Muons, Inc., Batavia, IL 60510, USA
[u] Visitor from Nagasaki Institute of Applied Science, Nagasaki, Japan
[v] Visitor from National Research Nuclear University, Moscow, Russia
[w] Visitor from University of Notre Dame, Notre Dame, IN 46556, USA
[x] Visitor from Universidad de Oviedo, E-33007 Oviedo, Spain
[y] Visitor from Texas Tech University, Lubbock, TX 79609, USA
[z] Visitor from Universidad Tecnica Federico Santa Maria, 110v Valparaiso, Chile
[aa] Visitor from Yarmouk University, Irbid 211-63, Jordan
[bb] On leave from J. Stefan Institute, Ljubljana, Slovenia

Diboson production ($WW + WZ + ZZ$) has been observed at the Tevatron in hadronic decay modes dominated by the WW process. This paper describes the measurement of the cross section of WZ and ZZ events in final states with large $\not\!\!E_T$ and using b-jet identification as a tool to suppress WW contributions. Because of the limited energy resolution, we cannot distinguish between partially hadronic decays of WZ and ZZ, and we measure the sum of these processes. The number of signal events is extracted using a simultaneous fit to the invariant mass distribution of the two jets for events with two b-jet candidates and events with fewer than two b-jet candidates. We measure a cross section $\sigma(p\bar{p} \to WZ, ZZ) = 5.8^{+3.6}_{-3.0}$ pb, in agreement with the standard model.

DOI: 10.1103/PhysRevD.85.012002 PACS numbers: 14.70.Fm, 12.15.Ji, 13.85.Qk, 14.70.Hp

I. INTRODUCTION

Measurements of diboson production cross sections provide tests of the self-interactions of the gauge bosons. Deviations from the standard model prediction for the production rates could indicate new physics [1,2], specifically in hadronic final states [3]. Furthermore, given that hadronic final states in diboson production are similar to associated Higgs boson production (Higgs-strahlung), $p\bar{p} \to VH + X$ ($V = W, Z$), the analysis techniques described in this paper are important for Higgs boson searches [4].

Diboson production has been observed at the Tevatron in fully leptonic final states [5,6]. In the case of partially hadronic decay modes, the CDF Collaboration observed a signal for combined measurement of WW, WZ, and ZZ using an integrated luminosity of 3.5 fb^{-1} where the signal is dominated by WW [7,8]. In this paper, we describe a measurement where we isolate the WZ and ZZ signals in partially hadronic decay channels by requiring the presence of b-jet candidates. We perform a fit to the dijet invariant mass spectrum (m_{jj}), splitting events into two nonoverlapping classes: with at least two b-jet candidates (two-tag channel) and fewer than two b-jet candidates (no-tag channel) [9]. This ensures maximum acceptance to the $WZ + ZZ$ events, and fitting in both the two-tag and the no-tag channel improves our signal sensitivity significantly compared to using only one channel (with or without b tagging). The signatures to which we are sensitive are $WZ \to \ell\nu b\bar{b}$ and $ZZ \to \nu\bar{\nu}b\bar{b}$ in the two-tag channel and all decays with unbalanced transverse momentum ($\not\!\!E_T$) in the no-tag channel ($WZ \to \ell\nu q\bar{q}$, $q\bar{q}'\nu\bar{\nu}$, and $ZZ \to \nu\bar{\nu}q\bar{q}$) [10].

II. THE CDF DETECTOR

The CDF II detector is described in detail elsewhere [11]. The detector is cylindrically symmetric around the proton beam axis which is oriented in the positive z direction. The polar angle, θ, is measured from the origin of the coordinate system at the center of the detector with respect to the z axis. Pseudorapidity, transverse energy, and transverse momentum are defined as $\eta = -\ln\tan(\theta/2)$, $E_T = E\sin\theta$, and $p_T = p\sin\theta$, respectively. The central and plug calorimeters, which, respectively, cover the pseudorapidity regions of $|\eta| < 1.1$ and $1.1 < |\eta| < 3.6$, surround the tracking system with a projective tower geometry. The detector has a charged particle tracking system immersed in a 1.4 T magnetic field, aligned coaxially with the $p\bar{p}$ beams. A silicon microstrip detector provides tracking over the radial range 1.5 to 28 cm. A 3.1 m long open-cell drift chamber, the central outer tracker, covers the radial range from 40 to 137 cm and provides up to 96 measurements with alternating axial and ±2° stereo superlayers. The fiducial region of the silicon detector extends to $|\eta| \sim 2$, while the central outer tracker provides coverage for $|\eta| \lesssim 1$. Muons are detected up to $|\eta| < 1.0$ by drift chambers located outside the hadronic calorimeters.

III. DATA SET AND EVENT SELECTION

We analyze a data set of $p\bar{p}$ collisions corresponding to an integrated luminosity of 5.2 fb^{-1} collected with the CDF II detector at a center-of-mass energy of 1.96 TeV. Events are selected via a set of triggers with $\not\!\!E_T$ requirements. The bulk of the data is collected with a trigger threshold $\not\!\!E_T > 45$ GeV. Other triggers have a lower $\not\!\!E_T$ requirement but also include additional requirements on jets in the event, or sometimes correspond to smaller effective integrated luminosity. We measure the trigger efficiency using an independent $Z \to \mu\mu$ sample and verify that the trigger logic used does not sculpt the shape of the dijet invariant mass.

Events with large $\not\!\!E_T$ ($\not\!\!E_T > 50$ GeV) and two or more jets are selected in this analysis. Jets are reconstructed in the calorimeter using the JETCLU cone algorithm [12] with a cone radius of 0.4 in (η, ϕ) space. The energy measured by the calorimeter is corrected for effects that distort the true jet energy [13]. Such effects include the nonlinear response of the calorimeter to particle energy, loss of energy in uninstrumented regions of the detector, energy radiated outside of the jet cone, and multiple proton antiproton interactions per beam crossing. The jets must have $E_T > 20$ GeV and be within $|\eta| < 2$. To suppress the multijet background contribution, we require the azimuthal angle between the $\vec{\not\!\!E}_T$ vector and any identified jet, $\Delta\phi(\vec{\not\!\!E}_T, \mathrm{jet})$, to be larger than 0.4 radians [14]. The $\not\!\!E_T$ significance, as defined in Ref. [7], measures the likelihood that the $\not\!\!E_T$ in the event comes from actual particles escaping detection as opposed to resolution effects and is typically low when $\not\!\!E_T$ arises from mismeasurements. We require $\not\!\!E_T$ significance to be larger than 4 (see Refs. [7,15]). Beam halo events are removed by requiring the event electromagnetic fraction, defined as the ratio between the amount of energy measured in the electromagnetic calorimeter and the sum of electromagnetic and hadronic calorimeter measurements, $E_{\rm EM}/E_{\rm total}$, to be between 0.3 and 0.85. We remove cosmic ray events based on timing information from the electromagnetic and hadronic calorimeters.

IV. SELECTING *b* QUARK JETS

To gain sensitivity to the b-quark content of our jet sample, we employ a new multivariate neural-network-based tagger that provides a figure of merit to indicate how b-like a jet appears to be. This tagger is unique in its emphasis on studying individual tracks. A more detailed description of this tagger may be found in Ref. [16]. The tagger identifies tracks with transverse momentum $p_T > 0.4$ GeV$/c$ that have registered hits in the innermost (silicon) tracking layers, and uses a track-by-track neural network to calculate a figure of merit for a given track's "b-ness", i.e., the likelihood that it comes from the decay of a B hadron. The observables used in the track neural network are the transverse momentum of the track in the laboratory frame, the transverse momentum of the track with respect to the jet axis, the rapidity with respect to the jet axis, and the track impact parameter with respect to the primary vertex and its uncertainty. The output of the track neural network is a numerical value in the range from -1 to 1.

Having the track b-nesses, we proceed to calculate the jet-by-jet b-nesses. We use tracks with track-by-track NN values greater than -0.5 in the fitting of a secondary vertex. The observables used as inputs to the jet neural network are the top five track b-nesses in the jet cone, the number of tracks with positive track b-ness, the significance [17] of the displacement of the secondary vertex from the B-hadron decay in the xy plane, the invariant mass of the tracks used to fit the displaced vertex, the number of K_S candidates found in the jet, and muon information for semileptonic B decays as described in Ref. [18]. We include the number of K_S candidates found since a much higher fraction of b jets than non-b jets contain K_S particles. The final output of the algorithm is a number between -1 and 1, the b-ness. By requiring values of b-ness closer to 1, one can select increasingly pure samples of b jets. The training for the track neural network as well as the jet-by-jet network is performed using jets matched to b quarks from $Z \rightarrow b\bar{b}$ events for signal and jets not matched to b quarks for background in a PYTHIA ZZ Monte Carlo (MC) sample.

To verify that the b-tagger data response is reproduced by the Monte Carlo simulation, we use two control samples, one dominated by $Z(\rightarrow \ell\ell) + 1$ jet events, and one dominated by $t\bar{t}$ pair events using a lepton + jets selection. The former offers a comparison of jets that largely do not originate from bottom quarks, while the latter compares jets in a heavily b-enhanced sample. We examine the b-ness distributions in simulation and data and use these comparisons to derive a correction to the tagging efficiency and mistag rates, the rate of misidentification of non-b jets as b jets, in the Monte Carlo simulation for the cuts on the jet b-ness that define our tagged selection. The operating point of our b tagger utilizes a tight cut on the highest b-ness jet in the event, and a looser cut on the second highest b-ness jet. We list the tagging efficiencies and mistag rates for these cuts in Table I. Further details of their determination are in Ref. [16]. We correct the MC, as it underestimates the observed mistag rate and overestimates the observed efficiency.

TABLE I. Mistag rates and efficiencies on jet b-ness cuts determined from comparisons of data and MC in our Z + jet and $t\bar{t}$ control samples. As we order jets in b-ness, the 1st jet is the highest b-ness jet in the event, and the 2nd jet is the 2nd highest b-ness jet in the event. The MC tends to overestimate the tagging efficiency and underestimate the mistag rate, and so we apply a correction.

		Data	Scale Factor on MC
Mistag Rate	1st jet	$1.00 \pm 0.21\%$	1.15 ± 0.24
	2nd jet	$8.19 \pm 0.34\%$	1.14 ± 0.05
Tag Efficiency	1st jet	$65.2 \pm 4.0\%$	0.95 ± 0.06
	2nd jet	$62.2 \pm 5.4\%$	0.91 ± 0.08

V. BACKGROUND ESTIMATION

We define our signal sample as events in the $40 < m_{jj} < 160$ GeV$/c^2$ region. In the calculation of the invariant mass m_{jj}, we use the two jets in the events with the highest b-ness score. The final number of events is extracted by a simultaneous fit to the dijet invariant mass distribution in the two-tag and no-tag channels, as defined above. Since we apply b tagging and allow for two or more jets, $t\bar{t}$ and single t production are a significant background. To further suppress these backgrounds, we require the events to have no more than one identified lepton (electrons or muons), where a very loose lepton identification is used to increase the efficiency of this rejection. In addition, the sum of the number of identified electrons, muons, and jets with $E_T > 10$ GeV must not exceed 4.

After this selection, we have four major classes of backgrounds:

1. Electroweak (EWK) V boson + jet processes that are estimated using Monte Carlo simulations and cross-checked using a γ + jets data set, described below.
2. Multijet events with generic QCD jet production which result in $\not\!\!E_T$ due to mismeasurements of the jet momenta. This background is evaluated using a data-driven method.
3. Single top and top-quark pair production. We estimate this background using a Monte Carlo simulation.

(4) $WW \to l\nu jj$ production. This is indistinguishable from the signal in the non-b-tagged region. This background is evaluated using a Monte Carlo simulation.

Monte Carlo simulations used for signal and background estimates are performed with a combination of PYTHIA [19], ALPGEN [20], and MADGRAPH [21] event generators interfaced with PYTHIA for parton showering. The geometric and kinematic acceptances are obtained using a GEANT-based simulation of the CDF II detector [22]. For the comparison to data, all sample cross sections are normalized to the results of next-to-leading order calculations performed with MCFM V5.4 program [23] and using the CTEQ6M parton distribution functions [24].

A. Multijet background

Multijet production does not typically contain large intrinsic $\not\!\!E_T$. The underlying assumption of how a multijet background event enters the analysis is that either jets are mismeasured, or that a charged or neutral hadron or a γ is lost in an uninstrumented region of the detector. We expect the dominant effect to be jet mismeasurement. Because of the high cross section of multijet production, this can be a significant background in a $\not\!\!E_T$ + jets-based analysis. We derive both the normalization and the dijet mass shape of the multijet background from data. The final measure of the amount of a multijet background will be determined from the extraction fit.

The two important cuts used to reject this background are on the $\not\!\!E_T$ significance and $\min[\Delta\phi(\vec{\not\!\!E}_T, \text{jet})]$. These distributions are shown in Fig. 1, which also demonstrates our ability to model the multijet background.

To estimate the remaining multijet background contribution, we construct a new variable, $\not\!\!p_T$, to complement the traditional calorimeter-based $\not\!\!E_T$. The $\not\!\!p_T$ is defined as the negative vector sum of tracks with $p_T > 0.3$ GeV$/c$.

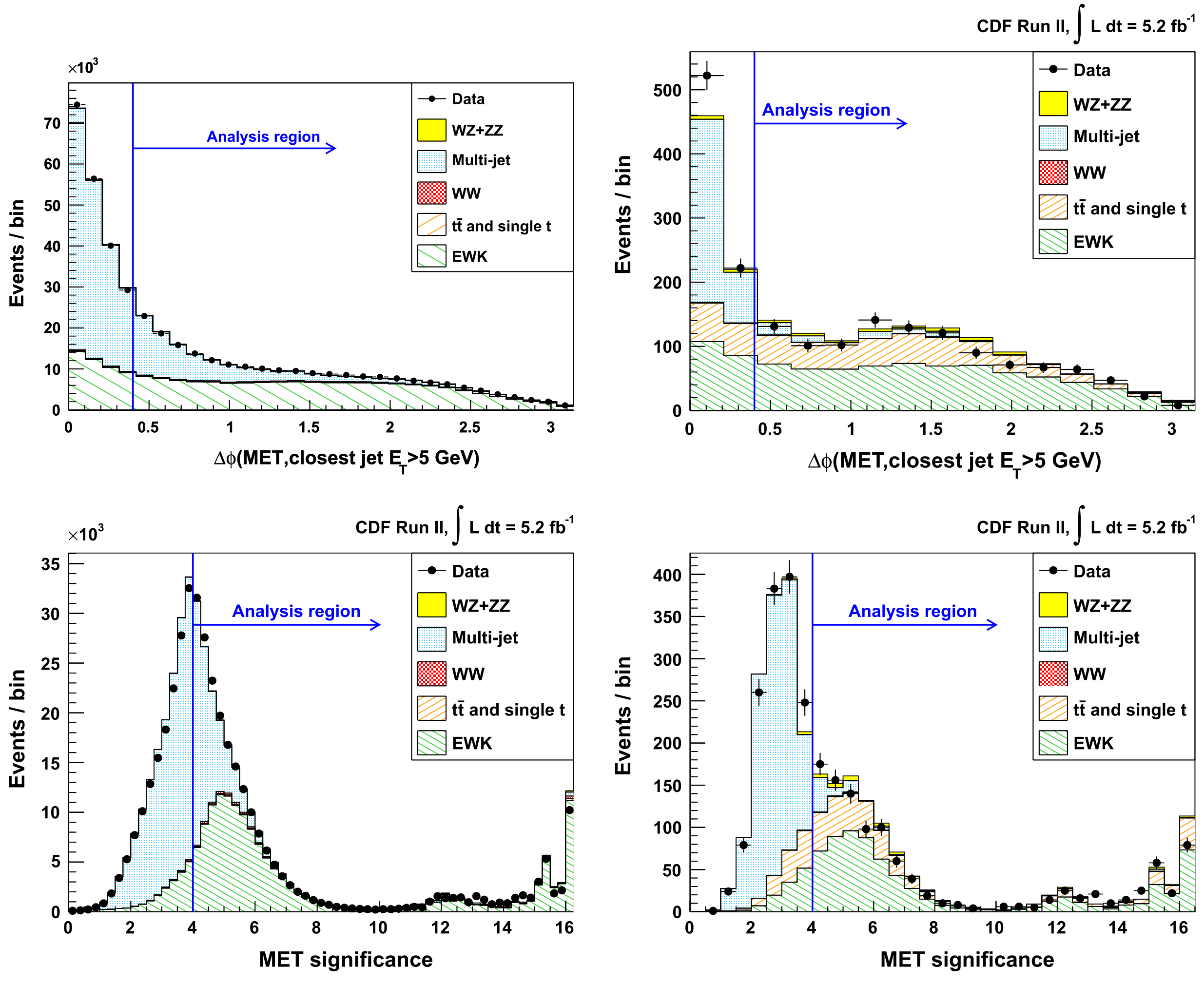

FIG. 1 (color online). *Left*: no-tag region. *Right*: 2-tag region. *Top row*: Minimum azimuthal angular separation $\min[\Delta\phi(\vec{\not\!\!E}_T, \text{jet})]$ between all jets with $E_T > 5$ GeV and the missing E_T, for events that pass all of the analysis cuts except for the $\min[\Delta\phi(\vec{\not\!\!E}_T, \text{jet})]$ cut. The analysis cut is at $\min[\Delta\phi(\vec{\not\!\!E}_T, \text{jet})] > 0.4$. *Bottom row*: $\not\!\!E_T$-significance distribution for events that pass all of the analysis cuts except for the $\not\!\!E_T$-significance cut. The analysis cut is at $\not\!\!E_T$ significance > 4. The highest bin is the overflow bin.

Tracks used in the calculation of $\not{p}_T$ have to pass minimal quality requirements and be within a $\pm 4\sigma$ window in the direction along the beam line from the primary vertex.

When comparing the azimuthal angle (ϕ) between $\not{E}_T$ and $\not{p}_T$, we expect the two quantities to align in the case of true $\not{E}_T$ (e.g., for diboson signal and electroweak backgrounds). The difference between these two angles is referred to as $\Delta\phi_{\mathrm{MET}}$. Electroweak backgrounds (and diboson signal) will be present in all regions, but will dominate at low $\Delta\phi_{\mathrm{MET}}$ due to correctly measured $\not{E}_T$ from neutrinos. To determine the dijet mass shape of the multijet background, we subtract all other background predictions obtained with Monte Carlo simulations from data, in the multijet enhanced region of $\Delta\phi_{\mathrm{MET}} > 1$. The normalization of the template obtained this way is then corrected to account for those events with $\Delta\phi_{\mathrm{MET}} \leq 1$. This correction introduces a 7% uncertainty on the normalization of the multijet background, where the uncertainty was assessed by obtaining the correction factor both in data and in a multijet Monte Carlo sample. The uncertainty on the shape of the distribution is estimated by comparing the difference in dijet mass shapes for $\Delta\phi_{\mathrm{MET}} > 1$ and $\Delta\phi_{\mathrm{MET}} < 1$ in a control sample defined by $3 < \not{E}_T$ significance < 4. The resulting multijet background dijet mass shape and its uncertainties are shown in Fig. 2 and are used as a shape uncertainty in the fit. For the two-tag channel, we do not have enough statistics to measure a shape, so we use the same shape as in the no-tag region.

B. Electroweak shape systematic

Following the method used in the $\not{E}_T$ + jets analysis of Ref. [7], we use a γ + jets data sample to check our modeling of the V + jet background shape. This is motivated by the similarities between the two types of processes. While there are some differences (the W and Z bosons are massive, the photon is not, and unlike the W, the photon lacks charge), these are accounted for by a weighting procedure described below.

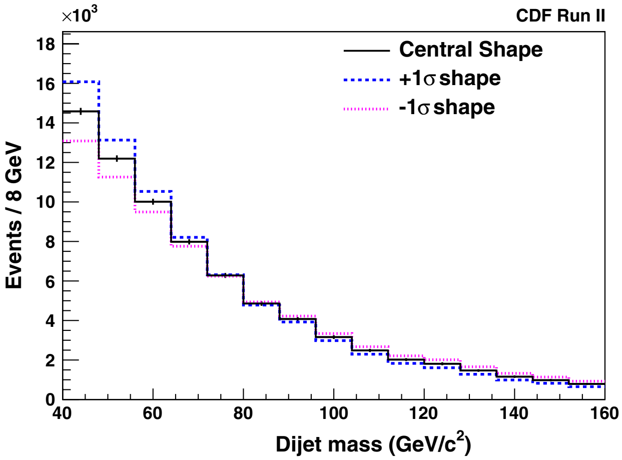

FIG. 2 (color online). The multijet background dijet mass template and its corresponding shape uncertainties.

TABLE II. List of differences between cuts applied to the $\not{E}_T$ + jets vs γ + jets sample. A "$\cdots$" denotes a lack of cut.

$\not{E}_T$ + jets	γ + jets
$\not{E}_T > 50$ GeV	$\lvert \vec{\not{E}}_T + \vec{\not{E}}_{T_{\mathrm{photon}}} \rvert > 50$ GeV
$\Delta\phi(\vec{\not{E}}_T, \mathrm{jet}) > 0.4$	$\Delta\phi(\vec{\not{E}}_T + \vec{\not{E}}_{T\mathrm{photon}}, \mathrm{jet}) > 0.4$
$0.3 < \frac{\mathrm{EM}}{E_{\mathrm{total}}} < 0.85$	$0.3 < \frac{\mathrm{EM}}{E_{\mathrm{total}}}$
$\not{E}_T$ significance > 4	$\cdots$
jet b-ness cuts	$\cdots$
$\cdots$	γ passes standard CDF cuts
$\cdots$	$\Delta R(\mathrm{photon, jet}) > 0.7$

Along with differences in the physics, there are also differences in the detector response to γ + jets and V + jets. In order to have the γ + jets events emulate the V + jets events, the photon E_T is vectorially subtracted from $\not{E}_T$. Doing this, the γ + jets becomes topologically very similar to the Z + jets with a Z decaying to neutrinos, or a W + jets with a W decaying to a neutrino and a missed or poorly reconstructed lepton. A few other differences exist in the selection cuts applied to γ + jets versus $\not{E}_T$ + jets data, shown in Table II. As with the different approach to $\not{E}_T$, these cuts are designed to allow for a data sample dominated by γ + jets events and having adequate statistics.

In order to account for those remaining kinematic differences between γ + jets and V + jets, we correct the γ + jets dijet mass shape in data based on the difference between γ + jets and V + jets Monte Carlo simulations. First, the ratio of the m_{jj} distributions from the V + jets Monte Carlo simulation and inclusive γ + jets Monte Carlo simulation is obtained. This ratio describes the difference in the physics of γ + jets and V + jets events. Note that since the γ + jets data sample will be contaminated with $\gamma + W/Z \rightarrow$ jets events peaking in the signal region, their expected contribution is subtracted from the γ + jets distribution. Next, the V + jets/γ + jets m_{jj} ratio histogram is multiplied bin-by-bin with the γ + jets data histogram, in effect sculpting the γ + jets data to look like V + jets data. Since the Monte Carlo simulated events enter only in the ratio, any production difference is taken into account while effects such as detector resolution, parton distribution function uncertainties, and modeling of initial- and final-state radiation cancel. After we apply this correction to the γ + jets data, there is a residual difference, shown in Fig. 3, between the corrected γ + jets data and our V + jets simulation, and we take this difference as a systematic uncertainty on the shape of the V + jets background prediction.

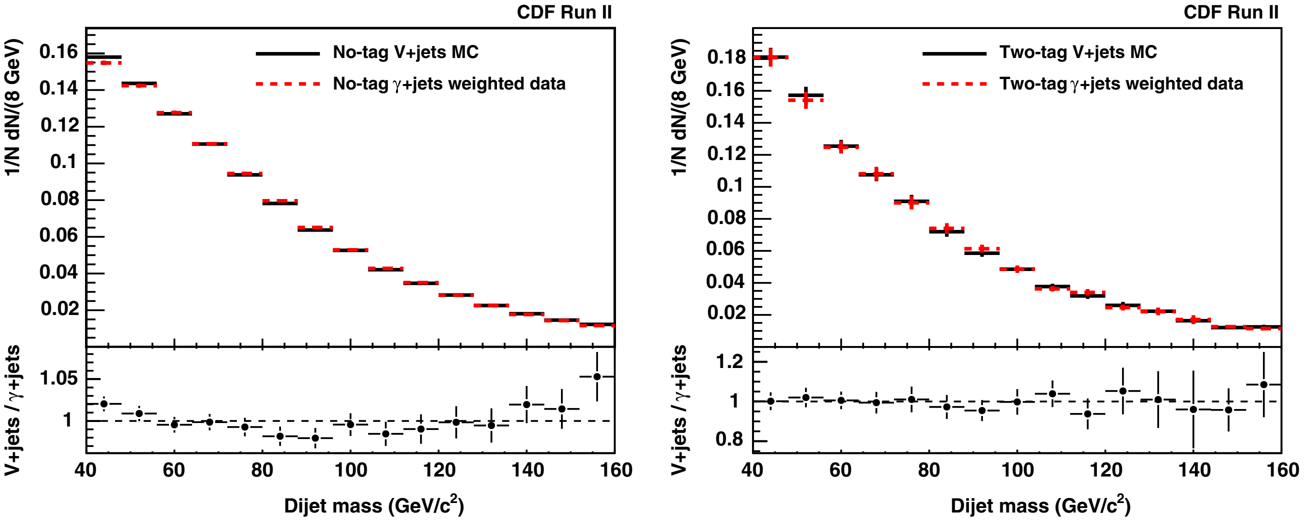

FIG. 3 (color online). Comparison of the γ + jets template with the electroweak MC template in the no-tag (left) and two-tag (right) regions.

VI. SIGNAL EXTRACTION AND RESULTS

We extract the number of signal events with a binned maximum likelihood fit to data using the method described in Ref. [25]. We supply template histograms for backgrounds and signals and perform a simultaneous fit in two channels, defined by different b-ness thresholds. The templates, and the uncertainties on their normalizations, are listed below:

(1) EWK background (W/Z + jets): Normalizations are allowed to float in the fit, unconstrained, with no correlation between the two tagging channels.

(2) $t\bar{t}$ and single top: The uncertainties on the theoretical cross sections of these processes are 6% [26] and 11% [27,28], respectively. We combine these two processes to a single template and treat these uncertainties as uncorrelated, which translates to an uncertainty of 5.8% on the normalization of the no-tag channel template, and 5.4% on the normalization of the two-tag channel template, due to the relative contributions of each process.

(3) Multijet background: We use our data-driven estimate, Gaussian constrained with an uncertainty of 7% in the no-tag channel. Because there are very few events in the two-tag channel template, we assign a normalization uncertainty equal to the statistical uncertainty ($\sqrt{N}/N$, 11%) of the template. The uncertainties in the two channels are treated as uncorrelated.

(4) WW: We use the next-to-leading order cross section and apply a Gaussian constraint to the number of WW events centered on this value with a width equal to the theoretical uncertainty of 6% [23].

(5) WZ/ZZ signal: As this is our signal, its normalization is allowed to float unconstrained in the fit. We assume that each signal process contributes proportionally to its predicted standard model cross section: 3.6 pb for WZ and 1.5 pb for ZZ ([23]), corrected for our selection's acceptance and efficiencies.

TABLE III. A summary of the systematic uncertainties incorporated into the fit of the dijet mass distribution. The cross section normalizations of the signal and EWK templates are allowed to float in the fit, unconstrained. There are additional uncertainties on the shape of the EWK and multijet templates, as described in the text. There is also an uncertainty on the shape of the diboson processes due to the jet energy scale. This shape uncertainty is correlated with the rate uncertainty shown here.

Systematic Uncertainties	channel	WZ/ZZ	WW	$t\bar{t}$ & single t	EWK	Multijet
Cross Section (Norm.)	no-tag	*Unconstrained*	±6%	±5.8%	*Unconstrained*	±7%
	2-tag	*Unconstrained*	±6%	±5.4%	*Unconstrained*	±11%
Jet Energy Scale	no-tag	±7.1%	±7.6%	±2.2%	···	···
	2-tag	±6.9%	±7.6%	±1.7%	···	···
b-ness cuts (up)	no-tag	+0.46%	+0.08%	+3.0%	···	···
	2-tag	−13.0%	−24.2%	−11.8%	···	···
b-ness cuts (down)	no-tag	−0.51%	−0.08%	−3.6%	···	···
	2-tag	+14.5%	+25.9%	+13.8%	···	···

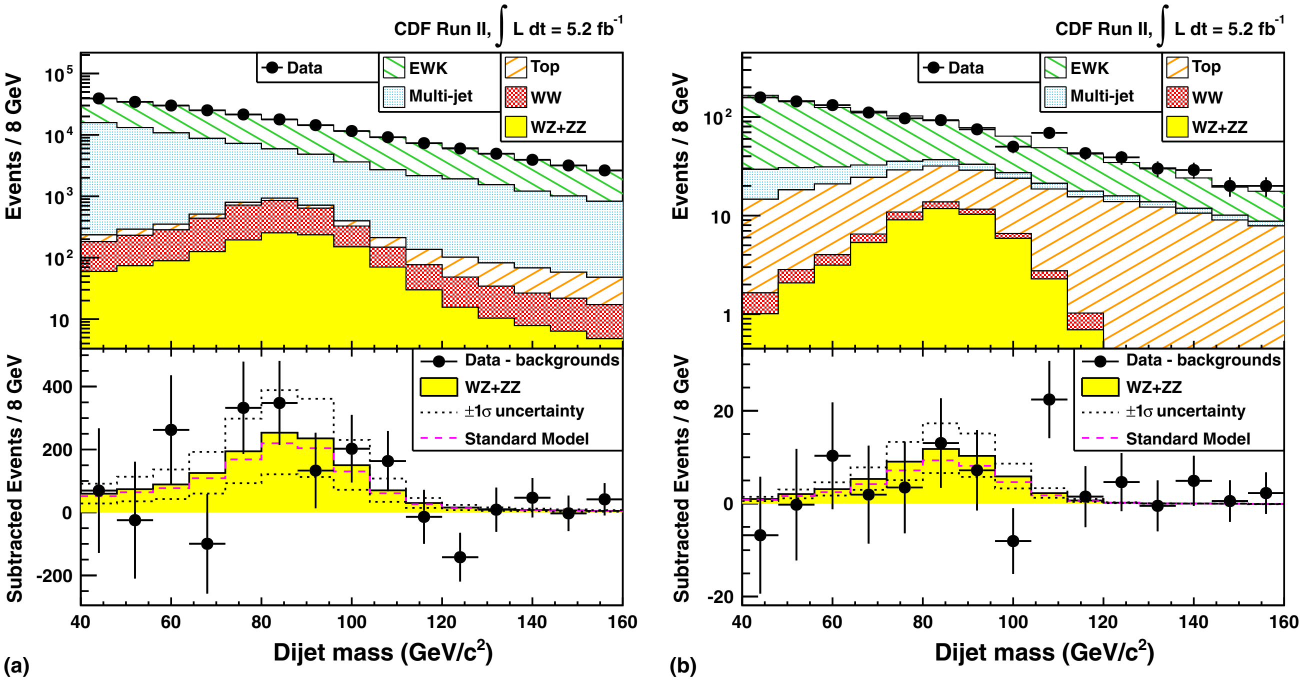

FIG. 4 (color online). Result of the fit to data for the double fit to all of WZ/ZZ. Left column is the no-tag channel; right column is the two-tag channel. Bottom row shows data after the background subtraction.

In addition to uncertainties on the normalizations of each template, we consider other systematic uncertainties that may affect the shape of templates. Shape uncertainties have been described for the electroweak and multijet backgrounds previously. For top and diboson samples, we consider the impact of the jet energy scale and the effect that uncertainties due to the differences between jet b-ness behavior in data and Monte Carlo simulation may have on the templates' shapes and normalizations. These uncertainties are summarized in Table III. All of the above uncertainties are treated as nuisance parameters and are incorporated into the fit using a Bayesian marginalization technique [25].

We choose the jet b-ness thresholds that define our two fitting channels to optimize the significance of our final result. The optimization for the two-tag channel points to a broad region where the sensitivity is maximized, and we choose the operating point for our b-ness thresholds in that region. The optimization favors that all remaining events be combined in a no-tag channel, rather than a single-tag channel with a low b-ness threshold. Figure 4 shows the results of the fit, and Table IV shows the number of fitted events.

TABLE IV. Extracted number of events from the 2-channel fit for WZ/ZZ, with all systematic uncertainties applied. Each uncertainty is reported to two significant figures, and all event totals are reported to the precision reflected in the uncertainty.

Process	Fit N_{events} (no-tag)	Fit N_{events} (two-tag)
EWK	$149\,900^{+5600}_{-5200}$	749 ± 48
$t\bar{t}$ and single t	898^{+59}_{-61}	217^{+23}_{-27}
Multijet	$76\,600^{+4900}_{-5300}$	76.3 ± 9.0
WW	2720 ± 200	$10.5^{+2.1}_{-2.3}$
WZ/ZZ	1330^{+710}_{-690}	52^{+24}_{-23}

To translate the result of our fit to the data to bounds or limits on the cross section of WZ/ZZ production, we construct Feldman-Cousins bands by analyzing the distribution of fitted (i.e., measured) cross sections in pseudoexperiments generated with a variety of scale factors on the input signal cross section [29]. When running pseudoexperiments, we consider the effect of additional systematic uncertainties that affect our acceptance. These are, in order of increasing significance: jet energy resolution (0.7%), $\not\!\!E_T$ modeling (1.0%), parton distribution functions (2.0%), initial and final-state radiation (2.4%), and luminosity and trigger efficiency uncertainties (6.4%). The set of input cross sections in our pseudoexperiments range from 0.1 to 3.0 times the standard model value with a step size of 0.1. Figure 5 shows the results of our Feldman-Cousins analysis. Based on a Monte Carlo simulation, the acceptance times efficiency for the WZ and ZZ production is 4.1%, and 4.6%, respectively.

Our measured result, using the 1σ bands from the Feldman-Cousins analysis, is $\sigma(p\bar{p} \to WZ, ZZ) = 5.8^{+3.6}_{-3.0}$ pb, in agreement with the standard model prediction $\sigma_{\text{SM}} = 5.1$ pb ([23]). We perform pseudoexperiments to calculate the probability (p value) that the background-only model fluctuates up to the observed result (observed p value) and up to the median expected $s + b$ result (expected p value). We observe a p value of 2.7%,

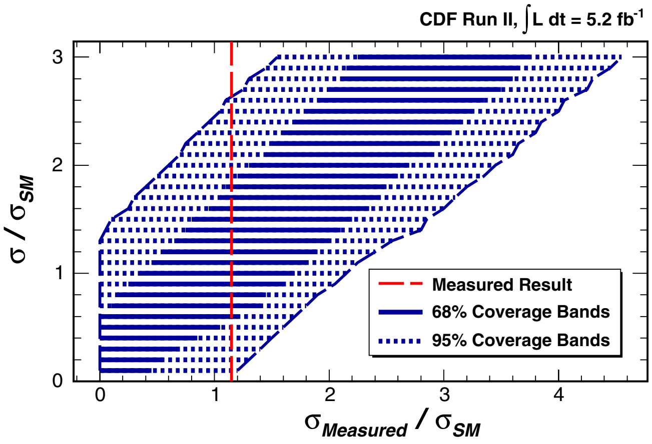

FIG. 5 (color online). Confidence bands showing the expected range of measured cross sections as a function of the true cross section, with 68% C.L. (blue solid region) and 95% C.L. (blue dotted region). Our measured result of $\sigma(p\bar{p} \to WZ, ZZ) = 5.8^{+3.6}_{-3.0}$ pb (red dashed vertical line) corresponds to a 95% C.L. at 13 pb ($2.6 \times \sigma_{\mathrm{SM}}$).

corresponding to a signal significance of 1.9σ where 1.7σ is expected. We set a limit on $\sigma_{WZ,ZZ} < 13$ pb ($2.6 \times \sigma_{\mathrm{SM}}$) with 95% C.L. The techniques used here, in particular, the *b* tagging algorithm, are being integrated in the current generation of searches for a low-mass Higgs boson.

ACKNOWLEDGMENTS

We thank the Fermilab staff and the technical staffs of the participating institutions for their vital contributions. This work was supported by the U.S. Department of Energy and National Science Foundation; the Italian Istituto Nazionale di Fisica Nucleare; the Ministry of Education, Culture, Sports, Science and Technology of Japan; the Natural Sciences and Engineering Research Council of Canada; the National Science Council of the Republic of China; the Swiss National Science Foundation; the A. P. Sloan Foundation; the Bundesministerium für Bildung und Forschung, Germany; the Korean World Class University Program, the National Research Foundation of Korea; the Science and Technology Facilities Council and the Royal Society, UK; the Institut National de Physique Nucleaire et Physique des Particules/CNRS; the Russian Foundation for Basic Research; the Ministerio de Ciencia e Innovación, and Programa Consolider-Ingenio 2010, Spain; the Slovak R&D Agency; the Academy of Finland; and the Australian Research Council (ARC).

---

[1] K. Hagiwara *et al.*, Nucl. Phys. **B282**, 253 (1987).
[2] M. Kober, B. Koch, and M. Bleicher, Phys. Rev. D **76**, 125001 (2007).
[3] E. J. Eichten, K. Lane, and A. Martin, Phys. Rev. Lett. **106**, 251803 (2011).
[4] T. Aaltonen *et al.* (CDF Collaboration), Phys. Rev. Lett. **104**, 141801 (2010).
[5] T. Aaltonen *et al.* (CDF Collaboration), Phys. Rev. Lett. **104**, 201801 (2010).
[6] V. M. Abazov *et al.* (D0 Collaboration), Phys. Rev. Lett. **103**, 191801 (2009).
[7] T. Aaltonen *et al.* (CDF Collaboration), Phys. Rev. Lett. **103**, 091803 (2009).
[8] T. Aaltonen *et al.* (CDF Collaboration), Phys. Rev. Lett. **104**, 101801 (2010).
[9] This last sample also contains *WW* events.
[10] We define the missing transverse momentum $\vec{\not\!\!E}_T \equiv -\Sigma_i E_T^i \mathbf{n}_i$, where $\mathbf{n}_i$ is the unit vector in the azimuthal plane that points from the beam line to the *i*th calorimeter tower. We call the magnitude of this vector $\not\!\!E_T$.
[11] A. Abulencia *et al.* (CDF Collaboration), J. Phys. G **34**, 2457 (2007).
[12] F. Abe *et al.* (CDF Collaboration), Phys. Rev. D **45**, 1448 (1992).
[13] A. Bhatti *et al.*, Nucl. Instrum. Methods A **566**, 375 (2006).
[14] All jets in the region $|\eta| < 3.6$ and $E_T > 5$ GeV are considered.
[15] M. Goncharov *et al.*, Nucl. Instrum. Methods A **565**, 543 (2006).
[16] J. Freeman, W. Ketchum, J. Lewis, S. Poprocki, A. Pronko, V. Rusu, and P. Wittich, Nucl. Instrum. Methods A **663**, 37 (2012).
[17] The significance of a quantity is defined as the value divided by its uncertainty.
[18] T. Aaltonen *et al.* (CDF Collaboration), Phys. Rev. D **79**, 052007 (2009).
[19] T. Sjöstrand *et al.*, J. High Energy Phys. 05 (2006) 026.
[20] M. L. Mangano *et al.*, J. High Energy Phys. 07 (2003) 001.
[21] J. Alwall *et al.*, J. High Energy Phys. 09 (2007) 028.
[22] R. Brun *et al.*, CERN Report No. CERN-DD-78-2-REV, 1978 (unpublished).
[23] J. M. Campbell and R. K. Ellis, Phys. Rev. D **60**, 113006 (1999).
[24] J. Pumplin *et al.*, J. High Energy Phys. 07 (2002) 012.
[25] T. Aaltonen *et al.* (CDF Collaboration), Phys. Rev. D **82**, 112005 (2010).
[26] U. Langenfeld, S. Moch, and P. Uwer, Phys. Rev. D **80**, 054009 (2009).
[27] N. Kidonakis, Phys. Rev. D **74**, 114012 (2006).
[28] N. Kidonakis, Proc. Sci. DIS2010 (2010) 196 [arXiv:1005.3330v1].
[29] G. J. Feldman and R. D. Cousins, Phys. Rev. D **57**, 3873 (1998).